J. Fluid Mech. (2013), *vol.* 731, R1, doi:10.1017/jfm.2013.388

JFM RAPIDS
journals.cambridge.org/rapids

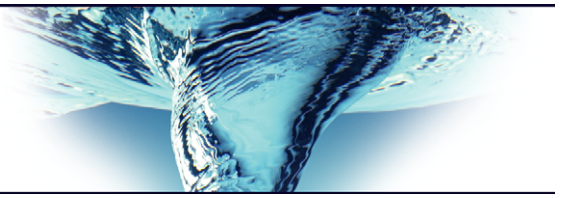

Turbulent spots in a channel: large-scale flow and self-sustainability

Grégoire Lemoult†, Jean-Luc Aider and José Eduardo Wesfreid

Laboratoire de Physique et Mécanique des Milieux Hétérogènes (PMMH), UMR CNRS 7636, ESPCI, UPMC, Paris Diderot, 10 rue Vauquelin, 75005 Paris, France

(Received 22 May 2013; revised 2 July 2013; accepted 24 July 2013;
first published online 14 August 2013)

Using a large-time-resolved particle image velocimetry field of view, a developing turbulent spot is followed in space and time in a rectangular channel flow for more than 100 advective time units. We show that the flow can be decomposed into a large-scale motion consisting of an asymmetric quadrupole centred on the spot and a small-scale part consisting of streamwise streaks. From the temporal evolution of the energy of the streamwise and spanwise velocity perturbations, it is suggested that a self-sustaining process can occur in a turbulent spot above a given Reynolds number.

Key words: channel flow, nonlinear instability, transition to turbulence

1. Introduction

Transition to turbulence in wall-bounded shear flows like plane Couette (PCF), Hagen–Poiseuille (HPF) or plane Poiseuille (PPF) flow and boundary layer flow occurs in the presence of localized coherent structures, known as turbulent spots. These objects, first discovered by Emmons (1951), are not composed of a single large-scale homogeneous structure, but of an assemblage of small-scale longitudinal vortices, separated from laminar flow by sharp fronts. For reviews of the subject see Riley & Gad-el Hak (1985), Henningson, Johansson & Alfredsson (1994) and Mathew & Das (2000).

The dynamics of a subcritical transition to turbulence, first observed in pipes by Reynolds (1883), is strongly related to the existence and interplay of these localized structures. Other isolated structures have been observed in a great variety of physical systems, such as thermal convection, magnetic liquids, granular material or buckling instabilities. Localized structures are related to subcritical instabilities, i.e. due to finite-amplitude perturbations (Knobloch 2008).

In the present study, we present an exhaustive description of turbulent spots in a rectangular channel, in a range of Reynolds numbers in which transition occurs. The

† Email address for correspondence: gregoire.lemoult@espci.fr

linear theory of stability predicts undisturbed stable laminar Poiseuille flow up to $Re = 5772$ (Orszag 1971), but experiments show transition at Reynolds numbers near $Re \approx 1300$ (Carlson, Widnall & Peeters 1982; Klingmann 1992; Lemoult, Aider & Wesfreid 2012), in the form of isolated turbulent spots.

Research on turbulent spots in channel flow has been performed with flow visualizations (Carlson *et al.* 1982; Alavyoon, Henningson & Alfredsson 1986), local measurements (Klingmann 1992; Seki & Matsubara 2012) and numerical simulations in both PPF (Henningson, Spalart & Kim 1987; Henningson & Kim 1991; Tsukahara, Seki, Kawamura & Tochio 2005; Aida, Tsukahara & Kawaguchi 2011; Takeishi *et al.* 2012) and PCF (Lundbladh & Johansson 1991; Schumacher & Eckhardt 2001; Lagha & Manneville 2007; Duguet & Schlatter 2013). To our knowledge, no experiments have been carried out on the detailed inner structure of the spots in a channel flow like those experimentally performed in pipe flow by van Doorne & Westerweel (2009), providing quantitative measurements of the full velocity field inside a turbulent spot.

Turbulent spots show transient growth, after which they either decay or are sustained, showing a complex spatio-temporal intermittent behaviour. Many questions remain open about the growth (streamwise expansion), the spreading (spanwise expansion) and the interaction of these turbulent domains, surrounded by laminar ones. The inhomogeneity of flow friction generates a coupling between the flow at the intermediate scale inside the turbulent domain and an external induced large-scale flow which can influence the morphology of turbulent spots. This topic has been studied theoretically and numerically, especially in PCF (see e.g. Schumacher & Eckhardt 2001; Lagha & Manneville 2007), but not yet observed experimentally. The spot spreading can be seen as a consequence of this large-scale flow as pointed out by Duguet & Schlatter (2013) in PCF in relation to the random nucleation of new streaks in the vicinity of the turbulent–laminar boundary (Duguet, Le Maître & Schlatter 2011). It has been observed in PPF that the leading and trailing edges of spots expand at different velocities (Carlson *et al.* 1982; Alavyoon *et al.* 1986) but the mechanism behind these observations remains unclear although there have been interesting suggestions in HPF. Shimizu & Kida (2009), Duguet, Willis & Kerswell (2010) and Hof *et al.* (2010) highlighted the local instability which occurs at the trailing edge as a driving mechanism of the spot. In certain cases, in PPF and PCF, turbulent spots show a complex spatio-temporal behaviour, including collective organization and branching in the form of bands (see e.g. Prigent *et al.* 2003; Tuckerman & Barkley 2011, and references inside).

Many theoretical efforts have attempted to understand the mechanisms sustaining the existence of turbulent spots. The non-normal linear stability theory explains that inner structures present maximum transient growth when they are oriented in the direction of the flow as streamwise streaks (Reddy & Henningson 1993; Trefethen *et al.* 1993). Linear stability theory also predicts the breakdown of these streaks (Reddy *et al.* 1998). However linear models fail to predict the existence of a sustained state in which laminar and turbulent areas coexist. A preferred framework for understanding this situation is provided by nonlinear models of self-sustained turbulence (Waleffe 1997; Shimizu & Kida 2009; Hall & Sherwin 2010; Barkley 2011). From these models, we expect that if sufficiently strong streamwise streaks are present inside the spots, a longitudinal wavy instability occurs. This instability will regenerate the initial streamwise streaks through a nonlinear mechanism. If this is the case, nonlinear amplification occurs, in time and space, inside the spot leading to a turbulent state.

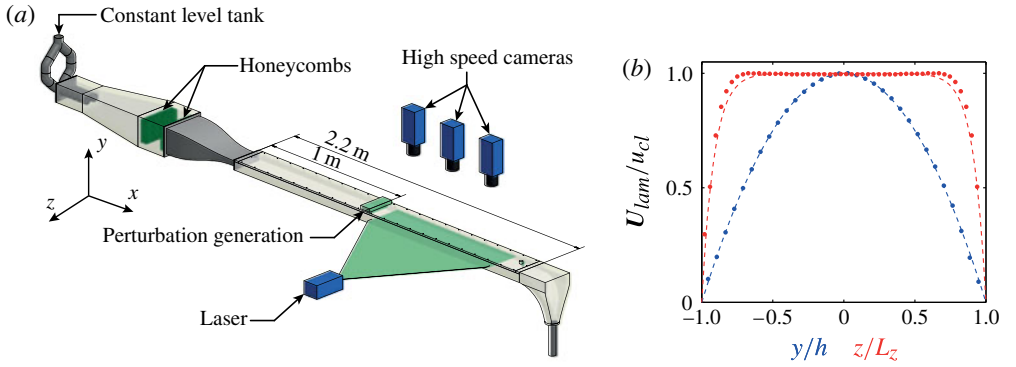

FIGURE 1. (*a*) Schematic view of the water channel (for details see Lemoult *et al.* 2012). The development section is 1 m long and the test section is 1.2 m long. Its cross-section is 20×150 mm^2. We use three synchronized high-speed cameras to measure the velocity field in the plane $y = 0.5h$ in a $(\Delta x, \Delta z) = (91h, 15h)$ area. (*b*) Laminar profile measured by PIV immediately after $x = 0$ for $Re = 2000$. Dashed lines are the theoretical profile and points are experimental data. In blue, profile measured in the $z = 0$ plane and in red, profile measured in the $y = 0$ plane.

The purpose of this article is to provide a precise experimental description of the flow field in and around a turbulent spot in PPF during its genesis and to discuss the relevance of the nonlinear process of self-sustainability.

2. Experimental set-up

The experimental system is composed of a 3 m long Plexiglas, constant-pressure-driven channel (figure 1). The test section half-height is $h = 10$ mm, its length is $220h$, and its width is $2L_z = 15h$. The Reynolds number, $Re = u_{cl}h/\nu$ (u_{cl} is the centreline velocity and ν the kinematic viscosity of the fluid), is estimated from volume flow measurements, assuming $u_{bulk} = (2/3)u_{cl}$. The x, y and z axes are, respectively, the streamwise, wall-normal and spanwise coordinates, with $y = 0$ in the middle of the channel and $(x, z) = (0, 0)$ where perturbations are injected. We define the advective time unit $t^* = t\,u_{cl}/h$ and the moving coordinate $x^* = x/h - t\,u_{bulk}/h$. The design of the inlet section, together with the smooth connections between all parts of the channel, minimize the upstream perturbations and keep the flow laminar up to $Re = 5500$, which corresponds to the maximum free-stream velocity of this channel. The perturbation is generated $100h$ downstream from the inlet to ensure a fully developed Poiseuille flow. Figure 1(*b*) shows the laminar profile measured by particle image velocimetry (PIV) immediately after $x = 0$ for $Re = 2000$. The parabolic velocity profile is recovered at $z = 0$ and the profile at $y = 0$ is flat in the range $-6h < z < 6h$.

The flow is perturbed by a round water jet normal to the flow, with diameter $d = 0.2h$, drilled into the upper wall. In the following, we will study the response of the flow to a single, short perturbation ($\Delta t = 150$ ms). The structure of the flow induced by the jet may be complex and depends strongly on the amplitude of the perturbation. Nevertheless, above a critical value and above $Re \approx 1300$, this small perturbation will always trigger the development of a turbulent spot (Lemoult *et al.* 2012).

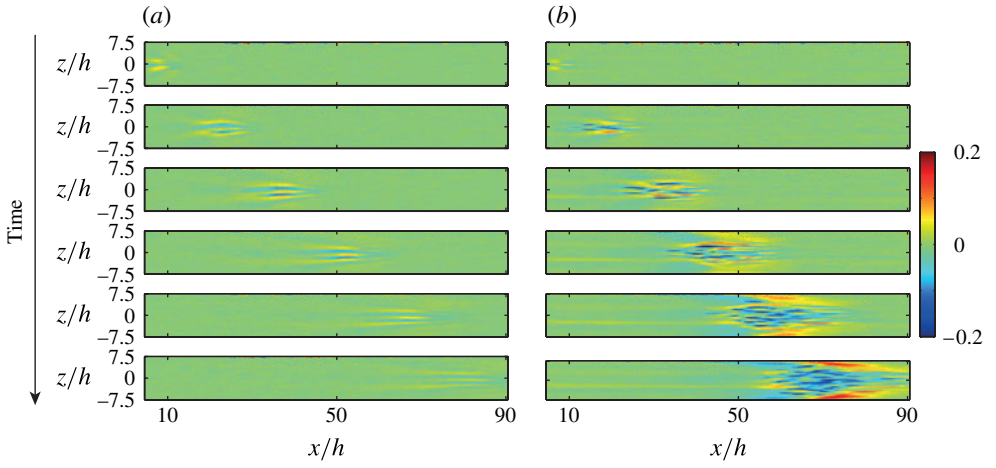

FIGURE 2. Temporal evolution of a developing turbulent spot visualized by its streamwise component u in a horizontal plane at $y = +0.5h$. Rows are, from top to bottom, respectively $t^* = 20$, 40, 60, 80, 100 and 120. For $Re = 1000$, (a), we observe the transient growth of the perturbation followed by its decay. On the other hand, for $Re = 3000$, (b), after an initial transient growth, the perturbation becomes sustained.

A time-resolved particle image velocimetry (TR-PIV) system is used to measure two-dimensional velocity fields (U, W) in the horizontal $y = +0.5h$ plane (figure 1). In the case of plane Poiseuille flow, the maximum streamwise fluctuations are expected near planes $y = \pm 0.5h$. The plane $y = +0.5h$ is preferred to $y = -0.5h$ due to the non-symmetric character of the injection (Klingmann 1992). The fluid is lit with a 1 mm thick light sheet and seeded with neutrally buoyant particles ($d_p \approx 20$ μm). In order to follow the spatial development of the perturbation as far as possible from the injection point, three adjacent synchronized high-speed cameras were used (figure 1). Using this set-up, the velocity field is measured over nearly the half-length of the channel. The measurement area is $5h < x < 91h$ and $-L_z < z < L_z$ and is mapped with $(N_x \times N_z) = (1721 \times 301)$ velocity vectors. The frame rate of the cameras has been adapted for each Re to ensure five frames per advective time unit.

3. Results and discussion

The measured velocity field $\boldsymbol{U} = (U, W)$ is decomposed as the sum of its laminar component $\boldsymbol{U}_{lam}$ and a perturbation $\boldsymbol{u}$. Figure 2 shows the time evolution of u for spots at $Re = 1000$ (figure 2a) and $Re = 3000$ (figure 2b). In addition to the advection of the perturbation by the mean flow, one can notice the streaky structure of the perturbation. The lower Re corresponds to a transient growth and the decay of the perturbation whereas the higher Re exhibits a sustained turbulent spot.

3.1. *Scale separation*

We define the spectral energy density $E_u(k)$ of the streamwise component u as follows. We first take the two-dimensional Fourier transform $\hat{u}(\boldsymbol{k})$ of u and transform it to polar coordinates with $k = 2\pi/\lambda = \sqrt{k_x^2 + k_z^2}$ and $\theta = \arctan(k_z/k_x)$, and then obtain a

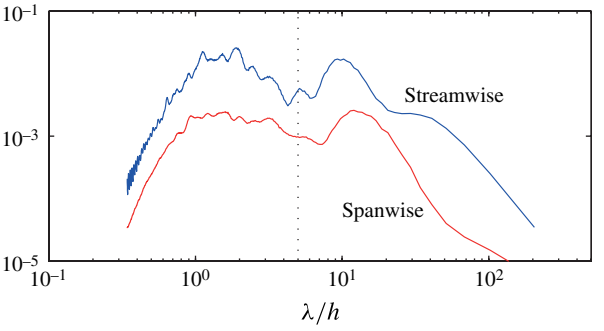

FIGURE 3. Azimuthally averaged pre-multiplied spectrum for streamwise $k\langle E_u(k)\rangle_t$ (blue) and spanwise component $k\langle E_w(k)\rangle_t$ (red) of the velocity field measure for $Re = 3000$. The spectrum is time averaged over $80 < t^* < 100$. The dotted line corresponds to $\lambda = 5h$ and delimits the large- and small-scale part of the flow.

spectrum azimuthally averaged over the angle θ by defining

$$E_u(k) = \int_0^{2\pi} |\hat{u}(\boldsymbol{k})|^2 k \, \mathrm{d}\theta \tag{3.1}$$

and analogously for the spanwise component w.

On figure 3, we present $k\langle E_u(k)\rangle_t$ and $k\langle E_w(k)\rangle_t$ for $Re = 3000$, where $\langle E_u(k)\rangle_t$ and $\langle E_w(k)\rangle_t$ are time averaged over $80 < t^* < 100$ in order to improve the signal-to-noise ratio. For sufficiently high Re, the flow can be decomposed into different scales, a large-scale flow ($\lambda > 5h$) and a small-scale flow ($\lambda < 5h$); this separation is indicated by the dotted line on figure 3. This observation justifies the decomposition of the fluctuating part of the flow into two components: the large-scale flow $\boldsymbol{u}_{large}$ and the small scale flow $\widetilde{\boldsymbol{u}}$. So that $\boldsymbol{U} = \boldsymbol{U}_{lam} + \boldsymbol{u}_{large} + \widetilde{\boldsymbol{u}}$

Using a fourth-order filter with a cut-off wavelength $\lambda_c = 5h$, the small-scale and large-scale structures of a turbulent spot are computed, and these are shown on figure 4. The small-scale flow is mainly formed of coherent low- and high-speed streaks whereas the large-scale flow corresponds to the generation of large-scale vertical vorticity Ω_y.

The large-scale flow is formed of a quadrupole centred on the spot. This large-scale flow is similar to that observed in PCF (see e.g. Schumacher & Eckhardt 2001; Lagha & Manneville 2007), except that the left–right symmetry is broken due to the mean advection. The turbulent area (which corresponds to the streaky flow) acts on the main flow as an obstacle and induces the large-scale flow. In return, the large-scale flow drives turbulent patches into the laminar area. This phenomenon seems to be responsible for the shape of spots observed by Carlson *et al.* (1982), Alavyoon *et al.* (1986) and Aida *et al.* (2011), and has been recently pointed out by Seki & Matsubara (2012) in PPF and by Duguet & Schlatter (2013) in PCF.

The large-scale flow computed here is obtained from a local measurement, in the $y = 0.5h$ plane, of the whole large-scale flow. Nevertheless, it has been checked that the quadrupole is also present in the $y = 0$ plane. It should also be present at $y = 0.5h$ due to the y-symmetry of the PPF. In consequence the y-averaged large-scale field should not be far from the field presented here. It is also important to notice that the relative small aspect ratio of the channel affects this large-scale flow. Due to the incompressible nature of the flow, it is expected that the large-scale flow in a wider

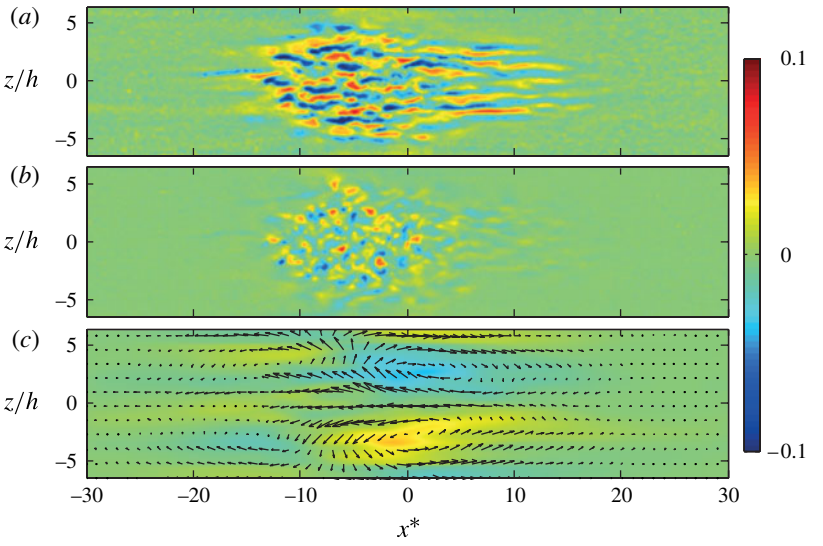

FIGURE 4. Instantaneous flow field at $t^* = 80$ for $Re = 3000$. (a) Small-scale streamwise velocity fluctuations $\widetilde{u}$, (b) small-scale spanwise velocity fluctuations $\widetilde{w}$ and (c) large-scale vorticity Ω_y, the arrows represent the large-scale flow field.

channel will be weaker, but still present, especially the accelerated areas at each side of the leading edge.

3.2. *Small-scale flow*

In the following, we focus on the small-scale flow $(\widetilde{u}, \widetilde{w})$ which corresponds to the turbulent part of the flow defined in the previous section.

Figure 5 presents the temporal evolution of the spanwise and streamwise spectra of $\widetilde{u}$ for different Re. Figure 5(a) ($Re = 1000$) shows that the energy is concentrated along streamwise modes with a wavenumber $k_z = 3h^{-1}$, which corresponds to a wavelength of $\sim 2h$. The flow is dominated by streaky structures, alternating between fast and slow streamwise streaks. These streaks are first generated by the initial perturbation, which induces a pair of quasi-streamwise counter-rotating vortices, before generating high- and low-streamwise-velocity streaks via the lift-up effect. This measurement is in accordance with previous measurements performed by Klingmann (1992). In the streamwise spectra, one can see that the energy is concentrated in the lowest wavenumbers. This is due to the spatial extension in the streamwise direction of the perturbation.

On the other hand, for higher Re, the turbulent spot can no longer be considered homogeneous: two different regions can be distinguished (figure 4 and supplementary movie 1 available at http://dx.doi.org/10.1017/jfm.2013.388). At the leading edge of the spot ($x > 0$), high and low speed streaks can be found, with the same wavenumber $k_z = 3h^{-1}$ as in the $Re = 1000$ case (figure 5). The upstream half of the spot ($x < 0$) presents more complicated structures exhibiting both streamwise and spanwise modes (figures 5b and 5c). These structures are a consequence of the destabilization of streamwise streaks in k_x modes. In our experiments it is difficult to discriminate between varicose and sinuous modes since the streaks are tangled. Nevertheless, both varicose and sinuous modes could be present since both are unstable (Waleffe 1997).

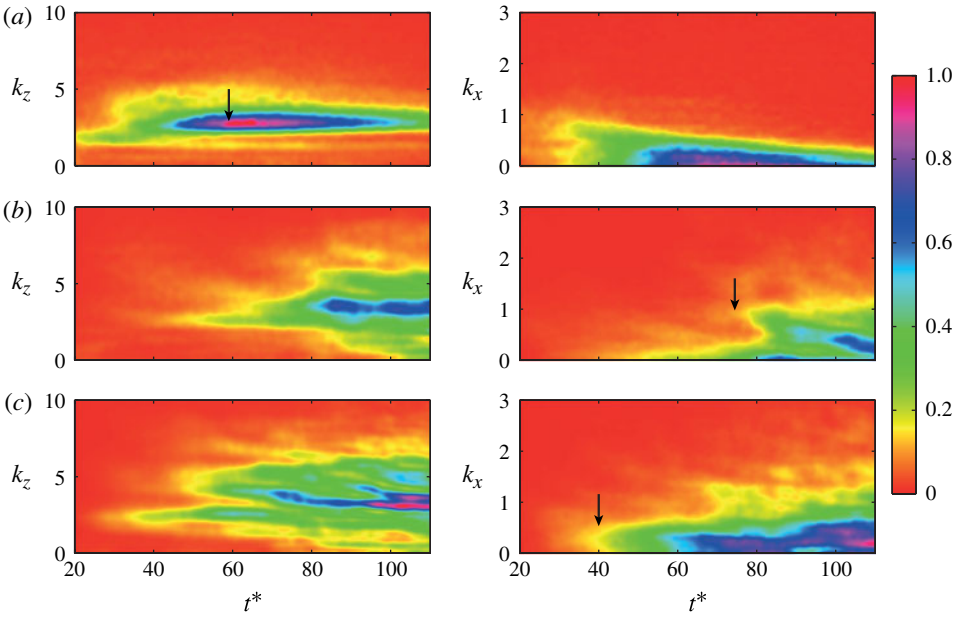

FIGURE 5. Temporal evolution of the streamwise and spanwise distribution of energy spectra for different Re (a, $Re = 1000$; b, $Re = 2000$ and c, $Re = 3000$). Each spectrum is scaled by its maximum. Arrow in (a) corresponds to the maximum of energy reached for t_{max}. Arrows in (b) and (c) correspond to the appearance of k_x modes.

3.3. *Temporal evolution*

In order to follow the emergence of such instabilities both in the streamwise direction and in time we define the following quantities:

$$E_{streaks}(x,t) = \frac{1}{2}\int_{-L_z}^{L_z} \widetilde{u}^2 \,\mathrm{d}z \quad \text{and} \quad E_z(x,t) = \frac{1}{2}\int_{-L_z}^{L_z} \widetilde{w}^2 \,\mathrm{d}z \tag{3.2}$$

$E_{streaks}(x,t)$ represents the kinetic energy associated with the streamwise component of the perturbation, basically the streaky flow, while $E_z(x,t)$ corresponds to the kinetic energy associated with the spanwise component of the flow at a given location along the channel.

Figure 6 presents the temporal evolution of the global spot energy integrated along x, $\langle E_{streaks}\rangle_x(t)$, for $Re = 1000$, 2000 and 3000. For each value of Re, we observe an initial increase of the energy. For $Re = 1000$, we measure $t_{max} = 58 \pm 2$, the time at which the spot energy reaches its maximum. This time can be compared to the measurements performed by Elofsson, Kawakami & Alfredsson (1999) and the prediction of Reddy & Henningson (1993). For $(k_x, k_z) = (0, 3)$, Reddy & Henningson (1993) found $t_{max} = 54$. This transient growth is explained by the non-normal nature of the Navier–Stokes operator linearized around the parabolic Poiseuille profile. Indeed, despite eigenvectors with negative real parts transient growth of finite-amplitude perturbations can occur (Trefethen *et al.* 1993). This transient growth is also observed for higher Re but for a specific time, t_{nonlin}, the energy shows a sudden increase. At this time the topology of the velocity field changes radically and k_x modes appear

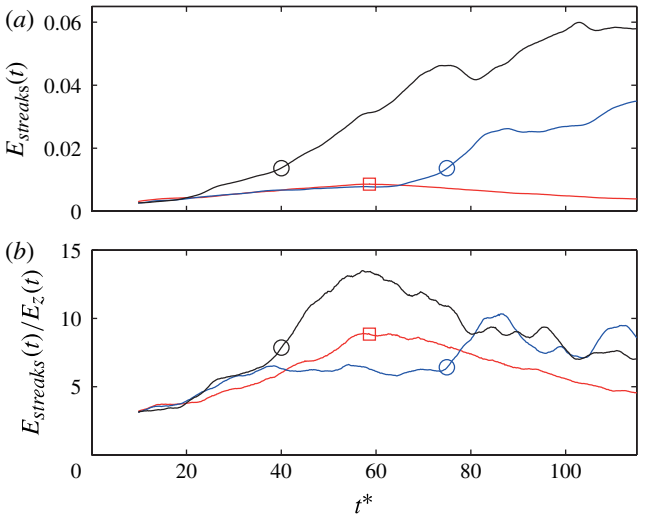

FIGURE 6. Temporal evolution of (*a*) the global energy associated with the streaks and (*b*) the ratio between the latter and the energy associated with the spanwise fluctuation. Red: $Re = 1000$, blue: $Re = 2000$ and black: $Re = 3000$. Squares represent the maximum in transient growth, t_{max}. Circles represent the appearance of nonlinear effects at t_{nonlin}.

Re	t_{max}	t_{nonlin}	$v_{E_{max}}$	$v_{trailing}$	$v_{leading}$
1000	58 ± 2	—	0.75 ± 0.02	—	—
2000	—	75 ± 2	0.66 ± 0.01	0.55 ± 0.01	0.84 ± 0.01
3000	—	40 ± 2	0.63 ± 0.01	0.50 ± 0.01	0.83 ± 0.01
4000	—	—	0.63 ± 0.02	0.47 ± 0.03	0.83 ± 0.05

TABLE 1. Summary of the results for different Re.

(figures 5 and 7). For $t* > t_{nonlin}$, the ratio $\langle E_{streaks} \rangle_x / \langle E_z \rangle_x$ becomes constant, suggesting a self-sustaining mechanism (Duriez, Aider & Wesfreid 2009).

Figure 7 presents the spatio-temporal evolution of local energies associated with the streamwise streaks and spanwise fluctuations for three Re in the frame moving at the bulk velocity. For $Re = 1000$ (figure 7*a*), it is possible to follow the position, $x_{E_{max}}$, of the kinetic energy maximum $E_{max} = E_{streaks} + E_z$ as a function of time. The velocity $v_{E_{max}} = \partial x_{E_{max}} / \partial t$ can be considered to be the group velocity of the perturbation. For $Re = 1000$, the perturbation travels slightly faster than the bulk velocity u_{bulk} since $v_{E_{max}} = 0.75 \pm 0.02$ (solid line in figure 7*a* and table 1). One can also observe an increase in the energy associated with streaks until t_{max}, which corresponds to the transient growth of the perturbation. Finally, this growth is not strong enough to trigger nonlinear mechanisms able to sustain turbulence and eventually we observe an exponential decay from t_{max}.

On figure 7(*b*), one can see that there is a drastic change for $Re = 2000$ compared to $Re = 1000$. After a short algebraic growth (see also figure 6) until $t_{nonlin} = 75 \pm 2$, we observe the increase of energy associated with spanwise fluctuations. This indicates that streaks which were already present in the flow become unstable. We also observe

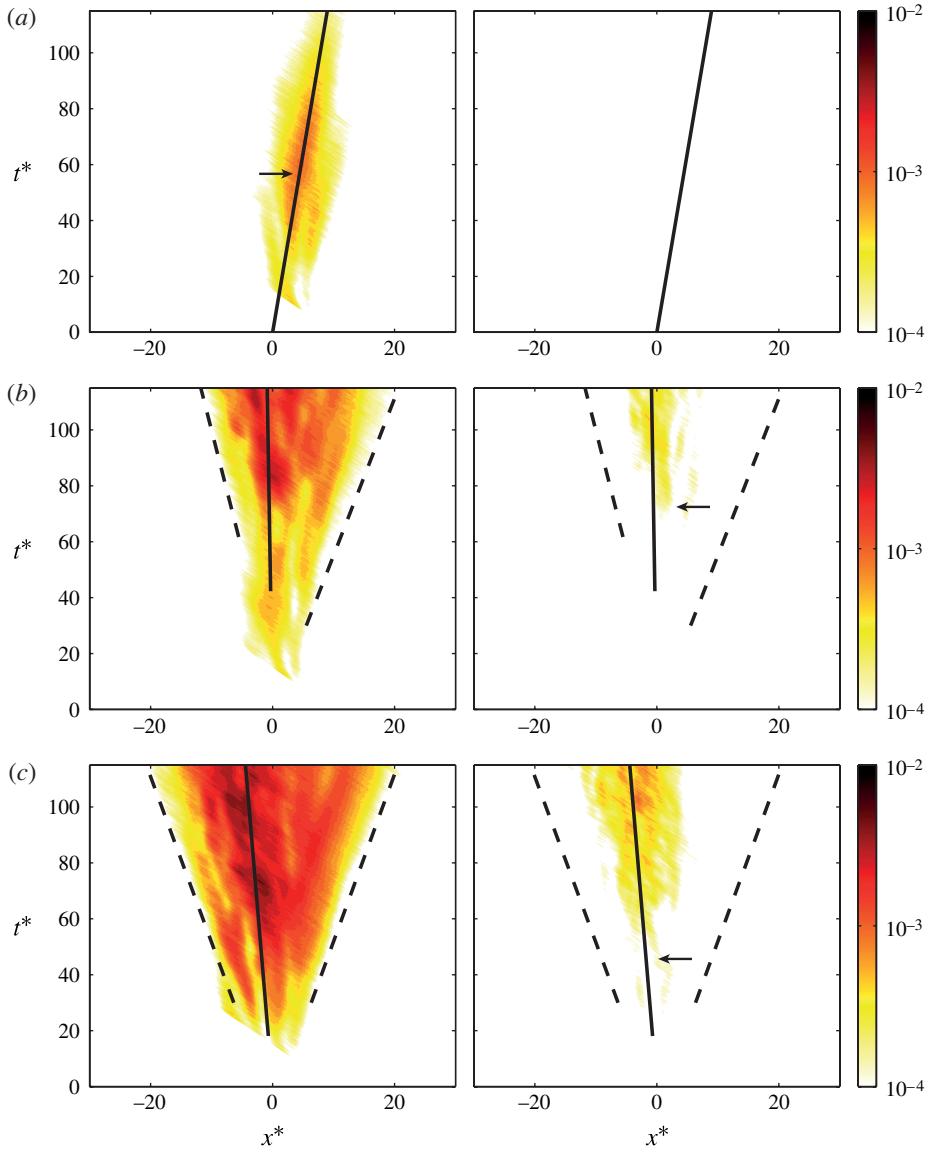

FIGURE 7. Spatio-temporal evolution of local energies associated with the streamwise streaks, $E_{streaks}(x^*, t)$ (left column) and spanwise fluctuations, $E_z(x^*, t)$ (right column) for different Re (a, $Re = 1000$; b, $Re = 2000$ and c, $Re = 3000$) in the frame moving at the bulk velocity. Solid line represents the fit by a linear function of the streamwise coordinate of the maximum of kinetic energy E_{max}. Dotted lines represent the fit by a linear function of the streamwise coordinate of the trailing and leading edge of the spot. Arrow in (a) corresponds to the maximum of energy reached for t_{max}. Arrows in (b,c) correspond to the appearance of energy associated with spanwise fluctuations.

the appearance of a trailing front which indicates a transition in the dynamics of the spot, underlined by the richness of the spectrum for $t > t_{nonlin}$ (figure 5). Note that this nonlinear phenomenon takes place in the upstream part of the spot ($x^* < 0$). The

downstream part of the spot is dominated by streamwise elongated streaks as can be seen in supplementary movie 1. These structures travel faster than the turbulent spot and are slowly damped by viscous effects.

The spatio-temporal diagram in figure 7(*c*) ($Re = 3000$) is similar to that obtained for $Re = 2000$. One can still see the development after a time $t_{nonlin} = 40 \pm 2$ of the energy associated to spanwise perturbations. The transient growth of the turbulent spot is masked by the earlier development of this nonlinear part of the flow compared to $Re = 2000$. The second notable difference is that the group velocity of the perturbation is smaller than the bulk velocity. The speed of the trailing edge is also smaller whereas the speed of the leading edge remains unchanged.

4. Conclusion

Using time-resolved PIV, we have followed the development of an induced perturbation in the subcritical regime in plane Poiseuille flow for more than 100 advective time units. From these measurements, we have been able to elucidate the process which governs the formation of a turbulent spot. First, a linear stage of transient growth and three-dimensional extension of the perturbation concentrates the energy into a well-defined spanwise mode with $\lambda = 2h$. This first stage is followed in the case of a sufficiently high Re by a nonlinear stage which involves the destabilization of the streaks previously formed and the redistribution of the energy into streamwise modes. The time evolution of energies associated with the streaks and with the spanwise fluctuations suggests the existence of a self-sustaining process in the turbulent spot.

We also have pointed out the separation of the flow into a small-scale motion, mainly composed of destabilized streamwise streaks, and a large-scale flow which surrounds the turbulent spot. This large-scale asymmetric quadrupole centred on the spot has been experimentally measured for the first time and could be responsible for the shape of the spot observed in visualization experiments (Carlson *et al.* 1982; Alavyoon *et al.* 1986) and numerically (Aida *et al.* 2011).

Acknowledgements

The authors would like to thank the DGA for its support. K. Gumowski is gratefully acknowledged for experimental assistance and D. Barkley and L. Tuckerman for helpful discussions.

Supplementary movie

A supplementary movie is available at http://dx.doi.org/10.1017/jfm.2013.388.

References

Aida, H., Tsukahara, T. & Kawaguchi, Y. 2011 Development of a turbulent spot into a stripe pattern in plane Poiseuille flow. In *Proceedings of Seventh Symposium on Turbulence and Shear Flow Phenomena, Ottawa, Volume 3*.

Alavyoon, F., Henningson, D. S. & Alfredsson, P. H. 1986 Turbulent spots in plane Poiseuille flow–flow visualization. *Phys. Fluids* **29**, 1328–1331.

Barkley, D. 2011 Simplifying the complexity of pipe flow. *Phys. Rev.* E **84**, 016309.

Carlson, D. R., Widnall, S. E. & Peeters, M. F. 1982 Flow-visualization study of transition in plane Poiseuille flow. *J. Fluid Mech.* **121**, 487–505.

VAN DOORNE, C. W. H. & WESTERWEEL, J. 2009 The flow structure of a puff. *Phil. Trans. R. Soc. Lond.* A **367**, 489–507.

DUGUET, Y., LE MAÎTRE, O. & SCHLATTER, P. 2011 Stochastic and deterministic motion of a laminar-turbulent front in a spanwisely extended Couette flow. *Phys. Rev.* E **84**, 066315.

DUGUET, Y. & SCHLATTER, P. 2013 Oblique laminar-turbulent interfaces in plane shear flows. *Phys. Rev. Lett.* **110**, 034502.

DUGUET, Y., WILLIS, A. P. & KERSWELL, R. R. 2010 Slug genesis in cylindrical pipe flow. *J. Fluid Mech.* **663**, 180–208.

DURIEZ, T., AIDER, J. L. & WESFREID, J. E. 2009 Self-sustaining process through streak generation in a flat-plate boundary layer. *Phys. Rev. Lett.* **103**, 144502.

ELOFSSON, P. A., KAWAKAMI, M. & ALFREDSSON, P. H. 1999 Experiments on the stability of streamwise streaks in plane Poiseuille flow. *Phys. Fluids* **11**, 915–930.

EMMONS, H. W. 1951 The laminar-turbulent transition in a boundary layer. *J. Aerosp. Sci.* **18**, 490–498.

HALL, P. & SHERWIN, S. 2010 Streamwise vortices in shear flows: harbingers of transition and the skeleton of coherent structures. *J. Fluid Mech.* **661**, 178–205.

HENNINGSON, D. S., JOHANSSON, A. V. & ALFREDSSON, P. H. 1994 Turbulent spots in channel flows. *J. Engng Maths* **28**, 21–42.

HENNINGSON, D. S. & KIM, J. 1991 On turbulent spots in plane Poiseuille flow. *J. Fluid Mech.* **228**, 183–205.

HENNINGSON, D. S., SPALART, P. & KIM, J. 1987 Numerical simulations of turbulent spots in plane Poiseuille and boundary-layer flow. *Phys. Fluids* **30**, 2914–2917.

HOF, B., DE LOZAR, A., AVILA, M., TU, X. & SCHNEIDER, T. M. 2010 Eliminating turbulence in spatially intermittent flows. *Science* **327**, 1491–1494.

KLINGMANN, B. G. B. 1992 On transition due to three-dimensional disturbances in plane Poiseuille flow. *J. Fluid Mech.* **240**, 167–195.

KNOBLOCH, E. 2008 Spatially localized structures in dissipative systems: open problems. *Nonlinearity* **21**, T45–T60.

LAGHA, M. & MANNEVILLE, P. 2007 Modelling of plane Couette flow. I. Large scale flow around turbulent spots. *Phys. Fluids* **19**, 094105.

LEMOULT, G., AIDER, J. L. & WESFREID, J. E. 2012 Experimental scaling law for the subcritical transition to turbulence in plane Poiseuille flow. *Phys. Rev.* E **85**, 025303.

LUNDBLADH, A. & JOHANSSON, A. V. 1991 Direct simulation of turbulent spots in plane Couette flow. *J. Fluid Mech.* **229**, 499–516.

MATHEW, J. & DAS, A. 2000 Direct numerical simulations of spots. *Curr. Sci.* **79**, 816–820.

ORSZAG, S. A. 1971 Accurate solution of the Orr–Sommerfeld stability equation. *J. Fluid Mech.* **50**, 689–703.

PRIGENT, A., GRÉGOIRE, G., CHATÉ, H. & DAUCHOT, O. 2003 Long-wavelength modulation of turbulent shear flows. *Physica* D **174**, 100–113.

REDDY, S. C. & HENNINGSON, D. S. 1993 Energy growth in viscous channel flows. *J. Fluid Mech.* **252**, 209–209.

REDDY, S. C., SCHMID, P. J., BAGGETT, J. S. & HENNINGSON, D. S. 1998 On the stability of streamwise streaks and transition thresholds in plane channel flows. *J. Fluid Mech.* **365**, 269–303.

REYNOLDS, O. 1883 An experimental investigation of the circumstances which determine whether the motion of water shall be direct or sinuous, and of the law of resistance in parallel channels. *Phil. Trans. R. Soc. Lond.* **174**, 935–982.

RILEY, J. J. & GAD-EL HAK, M. 1985 The dynamics of turbulent spots. In *Frontiers in Fluid Mechanics* (ed. S. H. Davis & J. L. Lumley), pp. 123–155. Springer.

SCHUMACHER, J. & ECKHARDT, B. 2001 Evolution of turbulent spots in a parallel shear flow. *Phys. Rev.* E **63**, 046307.

SEKI, D. & MATSUBARA, M. 2012 Experimental investigation of relaminarizing and transitional channel flows. *Phys. Fluids* **24**, 124102.

SHIMIZU, M. & KIDA, S. 2009 A driving mechanism of a turbulent puff in pipe flow. *Fluid Dyn. Res.* **41**, 045501.

TAKEISHI, K., KAWAHARA, G., UHLMANN, M., PINELLI, A. & GOTO, S. 2012 Puff-spot transition in rectangular-duct flow. In *Proceedings of JSST 2012 International Conference on Simulation Technology in Kobe, Japan*, p. 197.

TREFETHEN, L. N., TREFETHEN, A. E., REDDY, S. C. & DRISCOLL, T. A. 1993 Hydrodynamic stability without eigenvalues. *Science* **261**, 578–584.

TSUKAHARA, T., SEKI, Y., KAWAMURA, H. & TOCHIO, D. 2005 DNS of turbulent channel flow with very low Reynolds numbers. In *Proceedings of Fourth International Symposium on Turbulence and Shear Flow Phenomena, Williamsburg, Volume 3*, pp. 935–940.

TUCKERMAN, L. S. & BARKLEY, D. 2011 Patterns and dynamics in transitional plane couette flow. *Phys. Fluids* **23**, 041301.

WALEFFE, F. 1997 On a self-sustaining process in shear flows. *Phys. Fluids* **9**, 883–900.